JOURNAL OF VIROLOGY, Dec. 2010, p. 12665–12674 Vol. 84, No. 24
0022-538X/10/$12.00 doi:10.1128/JVI.00837-10

Interaction of Decay-Accelerating Factor with Echovirus 7▽

Pavel Plevka,[1]† Susan Hafenstein,[1,2]† Katherine G. Harris,[1] Javier O. Cifuente,[2] Ying Zhang,[1]‡ Valorie D. Bowman,[1] Paul R. Chipman,[1] Carol M. Bator,[1] Feng Lin,[3] M. Edward Medof,[3] and Michael G. Rossmann[1]*

Department of Biological Sciences, Purdue University, 915 W. State Street, West Lafayette, Indiana 47907-2054[1]; Department of Microbiology and Immunology, The Pennsylvania State University College of Medicine, 500 University Drive, Hershey, Pennsylvania 17033[2]; and Institute of Pathology, Case Western Reserve University, School of Medicine, 2085 Adelbert Road, Room 301, Cleveland, Ohio 44106[3]

Received 20 April 2010/Accepted 23 September 2010

Echovirus 7 (EV7) belongs to the *Enterovirus* genus within the family *Picornaviridae*. Many picornaviruses use IgG-like receptors that bind in the viral canyon and are required to initiate viral uncoating during infection. However, in addition, some of the enteroviruses use an alternative or additional receptor that binds outside the canyon. Decay-accelerating factor (DAF) has been identified as a cellular receptor for EV7. The crystal structure of EV7 has been determined to 3.1-Å resolution and used to interpret the 7.2-Å-resolution cryo-electron microscopy reconstruction of EV7 complexed with DAF. Each DAF binding site on EV7 is near a 2-fold icosahedral symmetry axis, which differs from the binding site of DAF on the surface of coxsackievirus B3, indicating that there are independent evolutionary processes by which DAF was selected as a picornavirus accessory receptor. This suggests that there is an advantage for these viruses to recognize DAF during the initial process of infection.

Echoviruses (EVs) belong to the family *Picornaviridae*, which contains some of the most common viral pathogens of vertebrates (43, 50, 51, 55, 58, 63). Picornaviruses are small, icosahedral, nonenveloped animal viruses. Their capsids have 60 copies each of four viral proteins, VP1, VP2, VP3, and VP4, that form an ~300-Å-diameter icosahedral shell filled with a positive-sense, single-stranded RNA genome. A distinctive feature of the capsid surface is a depression around the 5-fold axes of symmetry, called the "canyon" (47). The results of both genetic and structural studies have shown that the canyon is the site of receptor binding for many of these viruses (4, 11, 23, 25, 36, 47, 68), including echoviruses, which utilize β-integrins (6, 33, 66). Receptor molecules that bind in the canyon have been found to belong to the immunoglobulin superfamily (49). When these receptor molecules bind within the canyon, they dislodge a "pocket factor" within a pocket immediately below the surface of the canyon. The shape and environment of the pocket factor suggest that it might be a lipid (13, 32, 45, 54). When a receptor binds within the canyon, it depresses the floor of the canyon, corresponding to the roof of the pocket. Similarly, when a lipid or antiviral compound binds to the pocket, it expands the roof of the pocket, corresponding to the floor of the canyon (39, 45). Thus, receptors that bind to the canyon and the pocket factor compete with each other for binding to the virus. An absence of the hydrophobic pocket factor destabilizes the virus and initiates transition to altered "A" particles, a likely prelude to uncoating of the virion, possibly during passage through an endosomal vesicle (45).

Not all receptors of picornaviruses bind in the canyon. A minor group of human rhinoviruses (HRV) bind to the low-density-lipoprotein receptor family (17, 34, 61, 62), and some other picornaviruses, including certain coxsackie- and echoviruses, utilize decay-accelerating factor (DAF; also called CD55) as a cellular receptor (9, 28, 40, 52).

DAF is a member of a family of proteins that regulate complement activation by binding to and accelerating the decay of both classical and alternative pathway C3 and C5 convertases (7, 18, 26), the central amplification enzymes of the complement cascade. DAF is expressed on virtually all cell surfaces, protecting self cells from the immune system by rapidly dissociating any convertases that assemble, thereby halting the progression of a complement attack directed at the cell. Recent work (15, 27, 29, 56) has shown that DAF also participates in T-cell antiviral immunity (56) and protects against T-cell autoimmunity (29) by regulating complement that is produced locally by immune cells. The functional region of DAF consists of four short consensus repeats (SCR1, -2, -3, and -4). The structures have been determined for the SCR2-SCR3 fragment, the SCR3-SCR4 fragment, and the full four-domain region (30, 60, 65). Each of the SCR domains contains about 60 residues and is folded into a β structure stabilized by disulfide bridges. The four SCR domains form a relatively rigid extended rod with dimensions of 160 by 50 by 30 Å (30). The four domains rise about 180 Å above the plasma membrane, on a serine- and threonine-rich stalk of 94 amino acids, 11 of which are O-glycosylated, and is attached to the plasma membrane by a glycosylphosphatidylinositol (GPI) anchor.

Structural and genetic studies have shown that closely related picornaviruses have adapted to bind to DAF at different sites on the receptor surface (9, 31, 38, 42, 52, 64). Although DAF binding is likely to facilitate viral adsorption, the avail-

* Corresponding author. Mailing address: Department of Biological Sciences, Purdue University, 915 W. State Street, West Lafayette, IN 47907-2054. Phone: (765) 494-4911. Fax: (765) 496-1189. E-mail: mr@purdue.edu.

† P.P. and S.H. contributed equally to this study.

‡ Present address: Plexxikon Inc., 91 Bolivar Drive, Berkeley, CA 94710.

▽ Published ahead of print on 29 September 2010.

ability of DAF receptor molecules on the host is normally not sufficient for echovirus 7 (EV7) to enter cells. Presumably, viral adaptation to bind DAF offers some advantage to the virus, such as increasing the efficiency of infection.

In an earlier publication (14), a 16-Å-resolution cryo-electron microscopy (cryo-EM) density map of the EV7-DAF complex was interpreted with the homologous structures of coxsackievirus B3 (CVB3) for EV7 (74% sequence identity) and virus complement protein for DAF (25% sequence identity). Because of the limited resolution of the earlier cryo-EM reconstruction, it was concluded that DAF bound to EV7 by laying across the icosahedral 2-fold axes. This implied that there were two alternative DAF binding modes occupying the same site, but with DAF oriented in opposite directions, and that only one of these alternative sites could be occupied at a time. Here we describe an improved, 7.2-Å-resolution cryo-EM reconstruction of DAF bound to EV7 and 3.1-Å-resolution X-ray crystal structures of EV7. Together with previously determined structures of DAF (30), we now show that 2-fold axis-related DAF molecules bind close to the icosahedral 2-fold axes on the viral surface but (in contradiction to the earlier results and consistent with predictions made by Pettigrew et al. [38]) do not cross these axes. This is consistent with the results of DAF binding to EV12, which binds DAF similarly to the manner reported here and also predicted for EV7 (38). Thus, the binding modes of DAF to EV12 and EV7 are now shown to be similar, but not the same, and are completely different from the binding mode of DAF to CVB3.

TABLE 1. Scaling and refinement statistics

Parameter	Value or description[c]
Space group	P1
Unit cell dimensions (Å)	
A	297.1
B	297.7
C	300.6
α (°)	119.0
β (°)	100.1
γ (°)	108.4
Resolution limits (high-resolution bin) (Å)	25–3.1 (3.24–3.10)
Completeness (%)	46.1 (32.3)
R_{merge}[a]	9.2 (27.9)
Avg redundancy	1.2 (1.1)
$\langle I\rangle/\langle\sigma I\rangle$	5.95 (1.98)
Reciprocal space correlation coefficient of F_{obs} and F_{calc} after convergence of map	0.806 (0.579)
R factor	0.288 (0.366)
Avg B factor	25.6
% Ramachandran plot outliers[b]	0.7
% Most-favored regions in Ramachandran plot[b]	91.0
% Rotamer outliers[b]	0.8
RMSD for bonds (Å)	0.003
RMSD for angles (°)	0.95
No. of unique reflections	655,131

[a] $R_{merge} = \sum_h \sum_j |I_{hj} - \langle I_h\rangle| / \sum_h \sum_j |I_{hj}|$.
[b] According to the criteria of Molprobity (12).
[c] Values in parentheses are for the high-resolution bin.

MATERIALS AND METHODS

DAF and EV7 production. Human DAF was expressed in *Pichia pastoris* as a C-terminally His_6-tagged protein (14). The DAF construct consisted of the full-length ectodomain, containing SCR1, -2, -3, and -4 (amino acids 1 to 254), but lacked the serine-threonine-rich linker domain and the GPI anchor.

EV7 was propagated in rhabdomyosarcoma cells (RD cells) and purified as described previously (14). RD cells were brought to confluence in 150-mm-diameter plates at 37°C in Dulbecco minimal Eagle medium (DMEM) (Invitrogen) with 10% fetal bovine serum. The cells were rinsed with phosphate-buffered saline (PBS), followed by the addition of 5 ml of EV7 stock inoculum diluted in DMEM per dish, for a multiplicity of infection of 1 to 5. After incubation at 37°C for 1 h, 7 ml of fresh medium was added per dish and infection was allowed to progress for 48 h. Cells were harvested, pooled, and stored at −80°C.

Virus was purified by freezing and thawing the cells three times before adding NP-40 (1%). After homogenization, the preparation was centrifuged at 5,000 rpm for 10 min. $MgCl_2$ (to 5 mM), DNase (0.05 mg ml^{-1}), and SDS (to 0.5%) were added to the supernatant and incubated for 30 min at room temperature. Trypsin was added (0.5 mg ml^{-1}) and incubated for 10 min at 37°C. EDTA (10 mM) and sarcosine (1%) were added, and the pH was adjusted to neutral with NH_4OH. The virus was pelleted through 30% sucrose in 50 mM morpholineethanesulfonic acid (MES), pH 6.0, by centrifugation at 48,000 rpm for 2 h in a Beckmann 50.2 rotor. The pellets were resuspended in 50 mM MES, loaded onto 10 to 40% potassium tartrate–50 mM MES gradients, and centrifuged at 36,000 rpm for 90 min, using a Beckmann SW41 rotor. The virus bands were collected, diluted in 0.1 M NaCl, 20 mM Tris (pH 7.2) buffer, and pelleted by centrifugation at 48,000 rpm for 90 min, using a Beckmann 50.2 Ti rotor. Pellets were resuspended in 0.1 M NaCl, 20 mM Tris, pH 7.2. The virus concentration was estimated by measuring the absorbance at 260, 280, and 310 nm, assuming an extinction coefficient at 280 nm of 7.7 ml/cm · mg.

Crystallization and data collection. Crystals of EV7 were obtained by the hanging drop technique with a well solution containing 0.25% polyethylene glycol 8000 (PEG 8000), 0.25% glycerol, 400 mM NaCl, 150 mM $CaCl_2$, and 100 mM Tris, pH 8.0. The drops were prepared by mixing 5 μl of the well solution with an equal volume of virus solution. Crystals formed in about 7 days. For data collection, crystals were soaked for 30 to 90 s in mother liquor containing 12% PEG 400 and 19% glycerol and immediately frozen in liquid nitrogen. Data were collected from a single crystal at 100 K on the ADSC Quantum4 charge-coupled device (CCD) detector at beam line F1 at the Cornell High Energy Synchrotron Source. An oscillation range of 0.2° was used during data collection. The EV7 crystal diffracted to 3.1-Å resolution. Data (Table 1) were processed and scaled using the HKL2000 package (37).

X-ray structure determination. The EV7 crystals had a space group of P1. One virus particle occupied a crystallographic asymmetric unit, which in this case was the complete unit cell. Only three rotational parameters had to be determined to define the icosahedral symmetry of the particle, as the origin could be assigned arbitrarily. The locked self-rotation function in the program GLRF was used to identify the particle orientation (59), using reflections of between 10- and 4-Å resolution. The radius of integration was set to 290 Å. The results showed that the particle was rotated by a κ angle of 34.1° about an axis given by a φ angle of 78.6° and a ϕ angle of 36.7° from the standard icosahedral orientation when using the XYK polar angle convention. The CVB3 structure (Protein Data Bank [PDB] accession no. 1cov) was used to calculate initial phases for reflections to 10-Å resolution with the program CNS (8). The phases were refined with 15 cycles of 60-fold noncrystallographic symmetry averaging, using the program AVE (22). Phase information for higher-resolution reflections was obtained by extending the resolution one index at a time, followed each time by four cycles of averaging at the current resolution. This procedure was repeated until phases were obtained for reflections to 3.1-Å resolution. Particle orientation and unit cell parameters were refined by varying them in small steps and checking for the highest correlation coefficient after four cycles of phase refinement. The refined particle orientation was given by a rotation κ angle of 33.9° about an axis given by a φ angle of 78.8° and a ϕ angle of 36.9°.

The structure was built using the program O (21), starting from the CVB3 structure mutated to the EV7 amino acid sequence. The structure was refined by manual rebuilding alternating with coordinate and B-factor refinement in the program CNS. Noncrystallographic symmetry constraints were used during refinement. Other calculations were done using CCP4 (10). No water molecules were added because of the low resolution of the data.

Cryo-EM data collection and reconstruction. Full-length DAF molecules were incubated with EV7 at room temperature for 1 h at a ratio of four DAF molecules per potential binding site on the virus (240:1). Small aliquots of this mixture were applied to holey carbon-coated grids and vitrified in liquid ethane. Electron micrographs were recorded on Kodak SO-163 film by using a Phillips CM300 FEG microscope. Micrographs were digitized with a Zeiss Phodis microdensitometer at 7-μm intervals. The scans were averaged in boxes of 2 by 2

TABLE 2. EMfit comparison of fits of DAF models into DAF difference density[a]

PDB accession no.	R_{crit}	Sumf	Clash	−Den
1OJY-b	2.66	29.6	3.2	14.6
1OJY-a	**2.63**	**29.5**	**3.2**	**13.1**
1OJY-c	2.41	29.7	1.6	14.2
1OK3-a	2.33	29.7	4.0	13.9
1OJY-d	2.33	28.7	13.4	11.5
1OJW-b	2.32	30.4	26.3	7.2
1OK1-a	2.26	29.8	6.3	14.2
1OK2-a	2.25	29.6	3.9	14.2
1OK9-a	2.25	29.7	6.3	14.2
1OK3-b	2.25	29.9	21.3	14.7
1OJV-b	2.24	29.7	15.8	14.6
1OK1-b	2.24	30.2	27.7	11.9
1OJW-a	2.21	29.5	3.2	14.3
1OJV-a	2.20	29.4	4.7	14.2
1OK2-b	2.19	30.7	25.3	13.8
1OK9-b	2.14	30.2	26.0	12.6

[a] Sumf is the average value for the densities at atomic positions normalized by setting the highest density to 100. Clash is the percentage of atoms in the model that have clashes with symmetry-related protein molecules. −Den is the percentage of atoms positioned in negative density. R_{crit} is a weighted average of the differences from the mean values for the sumf, clash, and −den fit criteria, expressed as a ratio with respect to their standard deviations (48). The data in bold (1OJY-a) were used to interpret the difference density.

pixels. The final averaged pixel size was 2.69 Å. Approximately 15,000 complexed particles were selected and corrected for the contrast transfer function, using the program RobEM (http://cryoem.ucsd.edu/programs.shtm) to determine the amount of defocus, which ranged from 1.12 to 3.67 μm. The amplitudes and phases were modified by the observed phase-contrast function by an algorithm described at http://cryoem.ucsd.edu/programs.shtm. The reconstruction was started by combining projections down 2-, 3-, and 5-fold axes, using the software package Auto3dem. The EM reconstruction processes were performed using icosahedral averaging with the same software (67). The resolution of the resulting map was estimated as the resolution at which the correlation between the two sets of structure factors derived from calculating reconstructions with nonoverlapping half-data sets fell below 0.5. For the final three-dimensional reconstruction, data were included to a resolution at which the correlation between the Fourier coefficients of two independent data sets was higher than 0.3. Approximately 12,500 boxed particles were used to calculate the final reconstruction.

Difference map and fitting of the DAF structure into the cryo-EM density. The electron density corresponding to EV7 was superimposed onto the cryo-EM density based on the alignment of the icosahedral symmetry axes. The program EMfit was used to calibrate the exact magnification of the cryo-EM map of EV7 in complex with DAF by comparing it with a map derived from the crystallographically determined coordinates of EV7 (44). A "difference map" was calculated by masking out the density of the virus by setting to zero all grid points within 3 Å from any EV7 atom. The 16 available crystal structures of full-length DAF molecules (PDB accession no. 1OJV, 1OJW, 1OJY, 1OK1, 1OK2, 1OK3, and 1OK9) (30) were fitted into the difference map by using the program EMfit (Table 2) (48). Structures 1OJY-a and 1OJY-b achieved ~10% higher R_{crit} scores (Table 2) than the remaining DAF structures, indicating better fits into the difference density. Structure 1OJY-b had the highest R_{crit} score, but a small part of its SCR1 domain was positioned outside the density, as indicated by a higher −den score (percentage of atoms positioned in negative density) than that of 1OJY-a. Thus, the 1OJY-a structure was used to interpret the difference density.

Buried surface area and residues forming the protein-protein interface. The residues forming the DAF-virus interface were identified with the web service PISA (Protein Interfaces, Surfaces and Assemblies Service) of the European Bioinformatics Institute (http://www.ebi.ac.uk/msd-srv/prot_int/pistart.html) (24), based on buried surface area between the fitted DAF molecule and the capsid proteins. Special care was taken in checking the residues that formed the DAF-virus interface in cases when the fitted models clashed to ensure that only residues with meaningful relative locations were reported. The buried surface areas between the virus and individual DAF domains were also calculated using the PISA service.

Generation of a model of EV12. A homologous model of EV12 capsid proteins VP1, VP2, and VP3 was generated with the SWISS-MODEL web service (http://swissmodel/expasy.org/) (2), using the structure of EV11 as a starting template (PDB accession no. 1h8t) (57).

Protein structure accession numbers. The EV7 coordinates, together with the observed structure amplitudes, were deposited in the Protein Data Bank under accession number 2x5i. The reconstruction of the DAF-EV7 complex was deposited with the EM Data Bank under accession number EMD-5179. The coordinates of DAF and EV7 fitted into the cryo-EM reconstruction of the DAF and EV7 complex were deposited in the Protein Data Bank under accession number 3iyp.

RESULTS AND DISCUSSION

Quality of the structure. The crystal structure of EV7 was determined to 3.1-Å resolution. The electron density map resulting from 60-fold noncrystallographic averaging allowed building of the structure of the capsid proteins VP1, VP2, VP3, and VP4, except for residues 1 to 10 and 288 to 292 of VP1, 1 to 8 of VP2, and 16 to 23 of VP4. The mapping of individual residue positions was easy, and the interpretation of the density of the side chains was mostly straightforward because of the good quality of the electron density map. The structure of the icosahedral asymmetric unit consists of 828 amino acid residues and one lauric acid molecule. All measured reflections were used in the crystallographic refinement. If calculated, the R_{free} value would have been very close to the R value due to the high noncrystallographic symmetry (1). Basic structure quality indicators are listed in Table 1.

Coat protein fold and capsid structure. The EV7 virion has protrusions around 5-fold and 3-fold symmetry axes. The maximum radius of the particle is 165 Å. As is the case for all other known picornaviruses, the EV7 capsid proteins VP1, VP2, and VP3 have quasi-T=3 symmetry. VP1 molecules form pentamers around icosahedral 5-fold axes, whereas VP2 and VP3 form heterohexamers around icosahedral 3-fold axes (Fig. 1a). As in all other picornavirus structures, there is a hole along the 5-fold axes lined by hydrophobic residues. This hole is a consequence of the steric hindrance between the 5-fold axis-related VP1 subunits. The bottleneck is 5.6 Å in diameter, which is slightly smaller than those in coxsackievirus B3 (8.9 Å), human rhinovirus 1A (7.9 Å), and echovirus 11 (8.4 Å). The coat proteins VP1, VP2, and VP3 each form a "jelly roll" fold common to many icosahedral viruses. When the β-strands along the length of a polypeptide that is to be folded into a jelly roll structure are named BCDEFGHI, then the β-strands on the opposing β-sheets that make the β-sandwich have the sequences BIDG and CHEF. VP4 is a small protein that meanders from the 5-fold axis along the inner face of the protein shell formed by VP1, VP2, and VP3 toward the 3-fold axis.

The root mean square deviations (RMSD) between equivalent Cα atoms for EV1, EV7, EV11, CVB3, HRV14, and poliovirus 1 show that EV7 is most similar to EV11, with which it also has the highest sequence similarity (Table 3). The largest differences among the picornaviruses are located in loop regions exposed on the virion surface that are also the most important neutralizing immunogenic sites (13, 19, 47, 53). The variable regions of VP1 are the loops located around the 5-fold axes. In VP2, the most variable surface loop is the "puff" region formed by residues 129 to 180 (Fig. 1a). The EV7 puff is a prominent feature on the surface of the virus that lines the south rim of the canyon. The largest protrusion on the surface

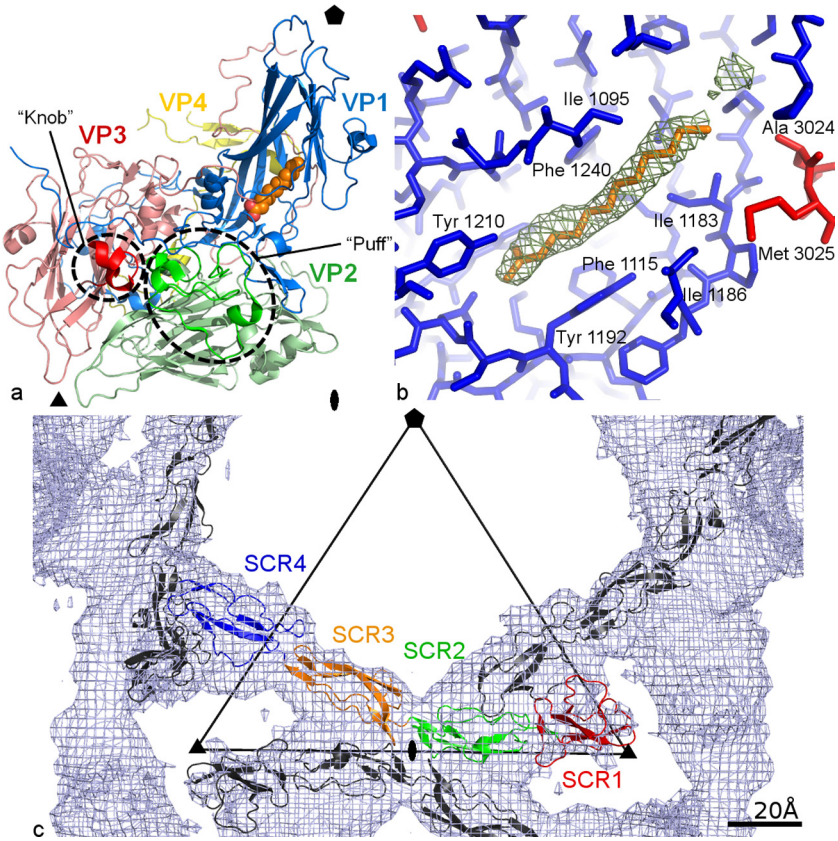

FIG. 1. Structures of EV7 and of DAF complexed with EV7. (a) Ribbon diagram of one protomer of EV7 showing VP1 (blue), VP2 (green), VP3 (red), VP4 (yellow), and the pocket factor (orange). Icosahedral symmetry elements are indicated. The puff and knob regions are outlined by dashed lines and shown with darker colors. (b) The pocket factor and its hydrophobic environment. The density corresponding to the pocket factor is shown in green, and the pocket factor (orange) is shown as a model of lauric acid. Most of the pocket is within VP1 (shown in blue, with residues labeled 1000 plus the sequence number), but it includes a few residues of VP3 (shown in red, with residues labeled 3000 plus the sequence number). (c) Cryo-EM difference density map representing DAF bound to EV7. One molecule of DAF is shown as a ribbon diagram with SCR1 (red), SCR2 (green), SCR3 (orange), and SCR4 (blue). Symmetry-related DAF molecules are shown in black. One asymmetric unit is indicated by a black triangular outline.

of the virus from VP3 is the "knob" (residues 58 to 69) (Fig. 1a). The puff and knob regions constitute most of the interface between DAF and EV7, as discussed below.

Pocket factor. A cavity in the VP1 β-barrel contains an elongated density which was assumed to be a pocket factor, as found in other rhino- and enteroviruses. The height of the pocket factor density was about three-fourths that of the surrounding protein density. However, the density was stronger close to the opening of the pocket and weaker and fragmented deeper in the pocket (Fig. 1b). Thus, probably not all 60 pockets in the virion are occupied, or different pockets contain moieties of different lengths. Alternatively, the fragmented density might represent a longer, labile hydrocarbon chain distal to the head group of the fatty acid. Since the EV7 pocket

TABLE 3. Sequence similarity and structural similarity in icosahedral asymmetric units of picornaviruses

Virus	Similarity with virus[a]					
	Poliovirus	HRV14	CVB3	EV11	EV1	EV7
EV7	0.99/96	1.06/95	0.64/98	0.56/99	0.68/97	
EV1	1.00/94	1.05/95	0.62/99	0.73/98		74
EV11	1.00/94	1.00/94	0.61/98		75	81
CVB3	0.98/96	1.01/94		77	75	74
HRV14	1.02/96		51	51	49	49
Poliovirus		50	57	56	56	56

[a] Values in the top left section of the table are RMSD (Å) for superimposed Cα atoms of the respective three-dimensional structures. The second number indicates the number of equivalent amino acids used to calculate the RMSD, expressed as a percentage with respect to the number of residues in the smaller of the two structures being compared. The icosahedral asymmetric unit consisting of subunits VP1, VP2, VP3, and VP4 was used as a rigid body in all cases. The program O (20) was used for superposition of the molecules. The cutoff for inclusion of residues for the RMSD calculation was 3.8 Å (46). Values in the bottom right section of the table are percent identities between the respective virus coat protein sequences. Gaps were ignored in the calculations.

TABLE 4. Comparison of numbers of residues that participate at protein-protein interfaces

Virus or proteins	No. of residues participating at the binding interface[a]							Total
	Coat proteins			DAF				
	VP1	VP2	VP3	SCR1	SCR2	SCR3	SCR4	
EV7	9	30	20	0	14	26	7	47
EV12	4	29	5	0	0	18	7	25
CVB3	20	20	15	0	26	9	10	45
Convertases	ND	ND	ND	0*	7*	8*	1*	16*

[a] ND, not defined. *, number of residues identified by mutagenesis studies to be important for interaction with classical and alternative convertases.

factor has not been identified, the continuous part of the density proximal to the pocket opening was modeled as a lauric acid molecule, a 12-carbon fatty acid (Fig. 1b). The polar group of lauric acid was placed into the higher density, close to the opening of the pocket in the canyon floor. The aliphatic chain extends along the pocket toward the icosahedral 5-fold axis. As in other picornaviruses (3, 16, 32), there are extensive interactions between the aliphatic chain and the side chains of the mostly hydrophobic residues that line the pocket (Fig. 1b). Most of the pocket is formed by VP1, but a small part close to the 5-fold axis is formed by VP3 (Fig. 1b).

DAF-EV7 complex. The cryo-EM image reconstruction of EV7 incubated with the SCR1-4 fragment of DAF was accomplished to 7.2-Å resolution. The absolute hand of the cryo-EM map was established by comparing the asymmetric features around the 2-fold symmetry axis with the crystallographic map of EV7. After setting all density corresponding to EV7 to zero, the remaining density was easily interpreted in terms of the four DAF domains (Fig. 1c). The mean height of the putative receptor density was about one-third of the mean height of the EV7 coat protein density. The lower height for DAF might represent a less-than-full substitution of DAF on the virus or an inaccurate contrast transfer function correction.

The ~50° bend between SCR1 and SCR2 of DAF established the N- to C-terminal direction of DAF in the difference map. Of the 16 DAF models that were available, the structure of DAF determined by Lukacik et al. (PDB accession no. 1OJY-a) (30) fitted the difference density best (Table 2). The 16 DAF models are identical in sequence but differ in structure. The biggest differences among the models are found in the angle between SCR domains 1 and 2. The fitting placed the connection between SCR2 and SCR3 close to the icosahedral 2-fold axis. It is therefore possible that there could be steric clashes between neighboring DAF molecules related by 2-fold symmetry. This might account for the less-than-full substitution of the DAF molecules. The DAF binding site is well away from the canyon, and thus DAF binding is unlikely to affect the pocket factor.

The structure of the EV7-DAF complex is similar to that of DAF bound to EV12. In both the EV7–SCR1-4 and EV12–SCR1-4 complexes, there was a diminution of the density representing DAF fragments, perhaps as a consequence of the steric hindrance across the icosahedral 2-fold axis. However, the lower density of DAF in the EV12–SCR3-4 complex could not have been caused by steric hindrance. Since the height of the DAF density in the EV7-DAF complex is only one-third that of the capsid density, it is possible that only one of the 2-fold axis-related sites is occupied at a time.

Docking of the known structure of DAF into the difference density resulted in two clashes, between atomic positions of residues 143 to 147 in SCR3 and residues 141 to 144 and 164 in VP2 and between atomic positions of residues 155 to 160 in SCR3 and residues 157 to 162 in VP2. Both of these clashes occur between SCR3 of DAF and the puff region of EV7. This might represent an inaccurate fitting result, but more probably it suggests a conformational change in DAF or EV7 in forming the complex. The average B factor for EV7 residues that clashed with DAF was 37.2 $Å^2$, whereas the average B factor for all of the atoms in the capsid was 25.6 $Å^2$. The situation was different for DAF. The average B factor for the 1OJY-a structure was 40.5 $Å^2$, and that for the atoms in residues that clashed with EV7 was 26.0 $Å^2$. Thus, the EV7 surface loops are more likely to change their conformation upon interaction of DAF with EV7. The higher B factor (corresponding to the average for molecules with greater conformational differences) for EV7 loops indicates that this region is more flexible and therefore might accommodate the structural changes induced by DAF binding. A similar situation occurred in the binding of DAF to CVB3, where the clash was between SCR2 and the puff region of the virus, suggesting that this flexible region on the virus surface is suitable for an induced-fit type of binding. Comparison of DAF binding to EV7 and CVB3 shows how structurally corresponding regions of two viruses adapted to bind to different parts of the DAF molecule.

Comparison of residues forming DAF binding sites in EV7, EV12, and CVB3. Buried surface area analysis was used to identify residues in the DAF-EV7 interface. To obtain consistent comparisons, it was therefore necessary to redetermine the residues in the interfaces of the DAF-EV12 and -CVB3 complexes. These comparisons also required calculation of a homology model of EV12 based on the known structure of EV11.

There are 59 capsid protein residues in EV7 that interact with the DAF molecule, but only 38 residues in EV12 (Table 4). The difference is caused mostly by the lack of any interaction of DAF SCR2 with EV12, whereas SCR2 interacts with 15 residues of EV7, providing an additional binding area of 400 $Å^2$. The interaction of SCR2 with EV7 but not with EV12 was demonstrated previously by biochemical analysis (38). The binding of EV7 to the extra DAF domain may increase the affinity of the virus for DAF. The buried surface areas between the SCR3 (900 $Å^2$) and SCR4 (350 $Å^2$) domains and EV7 are similar to those in the DAF-EV12 complex. Thirty of the residues of EV7 and EV12 that interact with DAF are located at equivalent positions in the capsid proteins, and among these, only seven are the same in both viruses (Fig. 2). Four of the

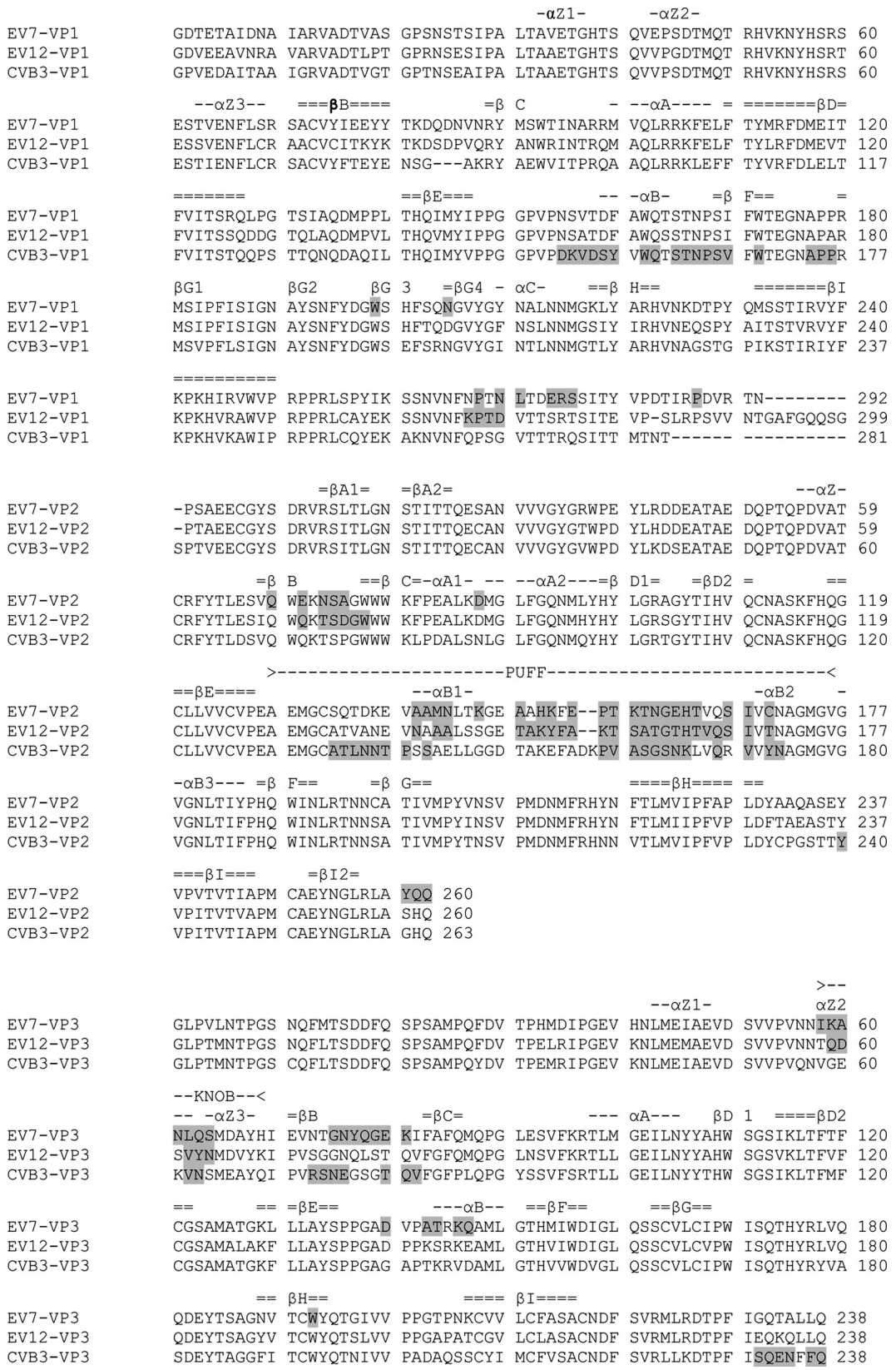

FIG. 2. Alignment of EV7, EV12, and CVB3 sequences. Secondary structural elements found in EV7 are shown across the top, and residues in contact with DAF are shaded.

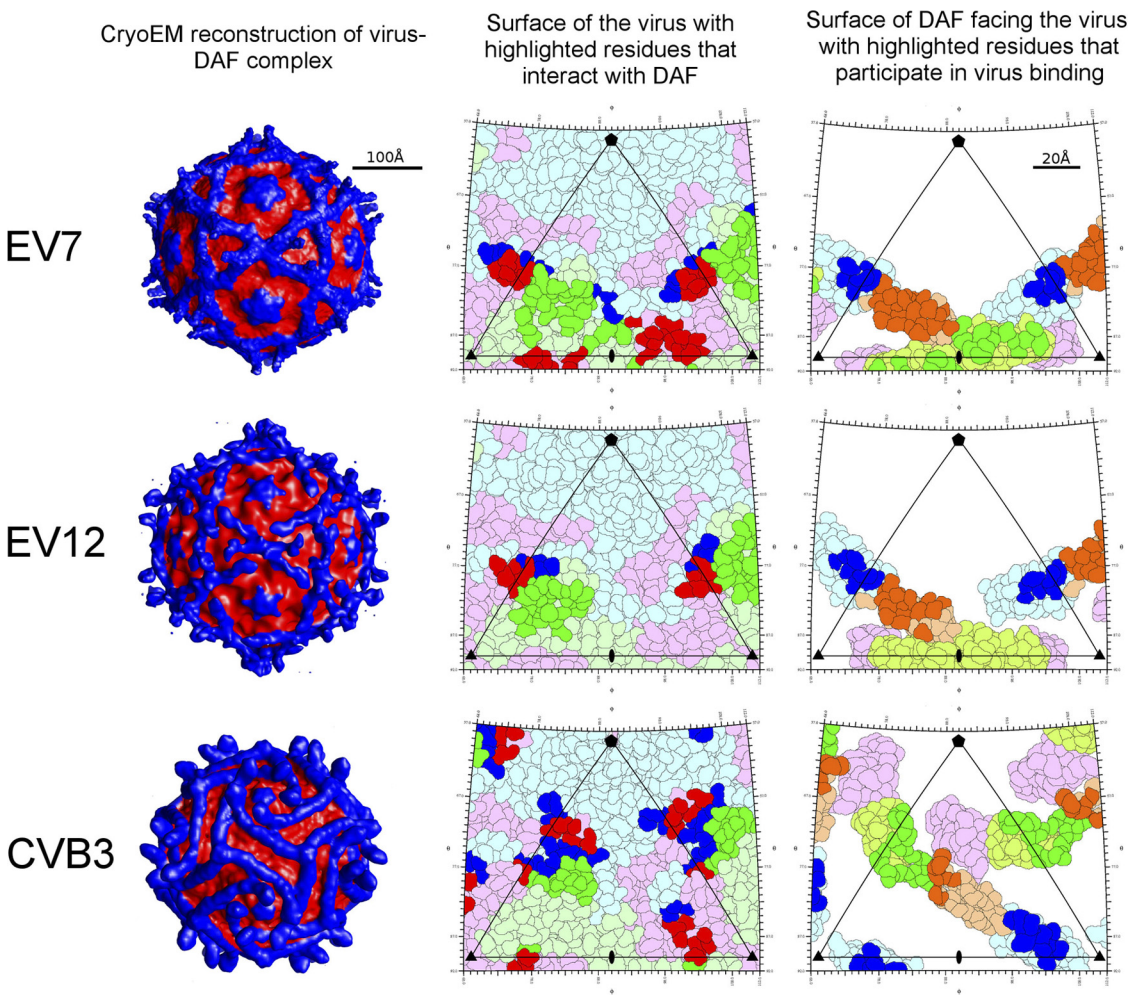

FIG. 3. Interaction of DAF with EV7, EV12, and CVB3. (Left) Surface-rendered view of each virus complexed with DAF, with all density at a radius of >160 Å shown in blue, which corresponds mostly to DAF density. (Middle) Outer surface of the virus, viewed from outside the virus and subdivided into small areas representing individual amino acids, with residues in VP1 shown in blue, those in VP2 shown in green, and those in VP3 shown in pink. Residues in contact with DAF are colored similarly, but in darker shades. (Right) Inner surface of DAF, viewed from inside the particle (with SCR1 residues in pink, SCR2 residues in green, SCR3 residues in orange, and SCR4 residues in blue), with DAF residues contacting the virus shown in darker shades. The asymmetric unit is indicated by a black triangular outline.

conserved residues are polar, and three are hydrophobic. All 7 residues are located in the VP2 subunit, and 6 of these are within a 12-residue stretch of the puff region. The seventh residue is only partly exposed on either virion. Of the six residues located in the puff region, Thr157, Gly161, His163, and Thr164 are well exposed on the surfaces of both viruses and also interact with the SCR3 domain of DAF. Thus, it is likely that these residues are important for DAF binding.

The site of binding and the type of contacts that CVB3 makes with DAF are completely different from those for DAF binding to EV7 and EV12 (Fig. 2 and 3). In CVB3, the DAF binding site is away from the icosahedral 2-fold axis and the principle contacts are between SCR2 and the virus. In all three DAF-virus complexes, SCR1 and SCR4 are located further from the surface of the virus than SCR2 and SCR3, and SCR1 makes no contact with the virus surface. Fifty-five CVB3 residues were identified to interact with DAF (Fig. 2). Only 19 and 11 residues of EV7 and EV12, respectively, that interact with DAF are located at positions structurally equivalent to those in CVB3 that bind to DAF (Fig. 2). Of these, only 1 and 2, respectively, are of the same type. Although there are some residues that are common to the DAF binding sites in EV7 (or EV12) and CVB3, residues from these sites interact with different DAF surfaces.

Comparison of DAF residues that bind to EV7, EV12, and CVB3. The buried surface area analysis identified 47 DAF residues that interact with EV7 and 25 that interact with EV12. Twenty-two of these residues are common to both interfaces (Fig. 4), indicating that the binding areas have extensive overlap. None of these residues are located in SCR2, 17 are in SCR3, and 5 are in SCR4. Thus, it appears that the interactions of DAF with EV7 and EV12 are conserved and are mostly within the SCR3 domain. This is in agreement with the location of the virus residues that bind DAF and that are the same in EV7 and EV12, i.e., within the VP2 puff region that binds to SCR3, as mentioned above.

```
                >---------------------------------SCR1---------------------------<
DAF - EV7       MQDCGLPPDV PNAQPALEGR TSFPEDTVIT YKCEESFVKI PGEKDSVICL KGSQWSDIEEF 61
DAF - EV12      MQDCGLPPDV PNAQPALEGR TSFPEDTVIT YKCEESFVKI PGEKDSVICL KGSQWSDIEEF 61
DAF - CVB3      MQDCGLPPDV PNAQPALEGR TSFPEDTVIT YKCEESFVKI PGEKDSVICL KGSQWSDIEEF 61
DAF - convert   MQDCGLPPDV PNAQPALEGR TSFPEDTVIT YKCEESFVKI PGEKDSVICL KGSQWSDIEEF 61

                 >---------------------------------SCR2-----------------------------------<
DAF - EV7        CNRSCEVPT RLNSASLKQP YITQNYFPVG TVVEYECRPG YRREPSLSPK LTCLQNLKWS TAVEFCKK 121
DAF - EV12       CNRSCEVPT RLNSASLKQP YITQNYFPVG TVVEYECRPG YRREPSLSPK LTCLQNLKWS TAVEFCKK 121
DAF - CVB3       CNRSCEVPT RLNSASLKQP YITQNYFPVG TVVEYECRPG YRREPSLSPK LTCLQNLKWS TAVEFCKK 121
DAF - convert    CNRSCEVPT RLNSASLKQP YITQNYFPVG TVVEYECRPG YRREPSLSPK LTCLQNLKWS TAVEFCKK 121

                       >---------------------------SCR3-----------------------------------<
DAF - EV7              KS CPNPGEIRNG QIDVPGGILF GATISFSCNT GYKLFGSTSS FCLISGSSVQ WSDPLPECRE 190
DAF - EV12             KS CPNPGEIRNG QIDVPGGILF GATISFSCNT GYKLFGSTSS FCLISGSSVQ WSDPLPECRE 190
DAF - CVB3             KS CPNPGEIRNG QIDVPGGILF GATISFSCNT GYKLFGSTSS FCLISGSSVQ WSDPLPECRE 190
DAF - convert          KS CPNPGEIRNG QIDVPGGILF GATISFSCNT GYKLFGSTSS FCLISGSSVQ WSDPLPECRE 190

                >-----------------------SCR4-----------------------------------------<
DAF - EV7       IYCPAPPQID NGIIQGERDH YGYRQSVTYA CNKGFTMIGE HSIYCTVNND EGEWSGPPPE CRGC 254
DAF - EV12      IYCPAPPQID NGIIQGERDH YGYRQSVTYA CNKGFTMIGE HSIYCTVNND EGEWSGPPPE CRGC 254
DAF - CVB3      IYCPAPPQID NGIIQGERDH YGYRQSVTYA CNKGFTMIGE HSIYCTVNND EGEWSGPPPE CRGC 254
DAF - convert   IYCPAPPQID NGIIQGERDH YGYRQSVTYA CNKGFTMIGE HSIYCTVNND EGEWSGPPPE CRGC 254
```

FIG. 4. Sequence of DAF, shaded gray where contacts are made with virus or convertase.

There are 45 DAF residues that interact with CVB3. The binding sites of DAF in CVB3 and EV7 overlap at only five residues within the SCR2 domain because the binding interfaces are on different sides of the DAF molecule (Fig. 5). The residues of DAF that interact with both viruses form a compact cluster on the surface of the DAF molecule (Fig. 5) but interact with different regions of the CVB3 and EV7 capsids (Fig. 3). In EV7, the residues interact with residues at the C termini of VP1 and VP2 and the EF loop of VP3 that are located at the edge of the depression at the 2-fold icosahedral axis. In CVB3, the five DAF residues interact with the puff region of VP2, approximately between the icosahedral 3-fold, 2-fold, and 5-fold axes. Different types of virus residues interact with the five common DAF residues in the DAF-EV7 and DAF-CVB3 complexes. There is no overlap between the surfaces by which DAF binds to CVB3 and EV12.

Seventeen DAF residues were shown to be important for regulation of classical and alternative pathway convertases (7, 18, 26) (Fig. 4). Different sets of six residues that regulate convertase activity are part of the EV7 and CVB3 binding interfaces, whereas only one of these residues is part of the EV12 interface. Specific binding of a virus to DAF residues that are important for complement regulation could be beneficial for the virus, as these residues are likely to be conserved because mutations would decrease the ability of DAF to protect cells from complement attack.

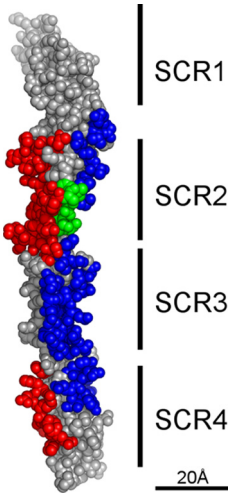

FIG. 5. Space-filling model of DAF showing contacts with EV7 (blue) or CVB3 (red) and the residues involved in contacting both EV7 and CVB3 (green).

Convergent evolution toward the use of DAF as a receptor molecule. Sequence comparisons have shown that coxsackieviruses and echoviruses have a common evolutionary origin and that EV7 and EV12 are more closely related to each other than to CVB3 (35). It has been shown by mutational analyses (5, 9, 38, 41, 42) that DAF binds in various ways to the surfaces of different EVs. The binding of DAF to CVB3 is completely different from that to the echoviruses. Because of the lack of relationship in the binding of DAF, it is more likely that the DAF binding abilities of CVB3 and the echoviruses were acquired independently than that the two binding mechanisms evolved from a common starting point. This indicates convergent evolution toward the use of the same receptor, presumably because binding of the virus to DAF gives some advantage, such as increasing the efficiency of infection. It is possible that the long and exposed surface binding area of DAF is a more efficient way for the virus to attach to a cell than the far more limited binding area of immunoglobulin-like cell surface adhesion molecules. Thus, the adaptation of different surface parts of homologous viruses to bind the same receptor molecule is a more recent evolutionary event than the divergence of these viruses from each other. A similar situation occurred in the use of different receptors to bind to more anciently diverged rhinoviruses (61).

ACKNOWLEDGMENTS

We thank Marc Morais, Shee-Mei Lok, and Bärbel Kaufmann for helpful advice. We thank Sheryl Kelly for help with the preparation of the manuscript.

This work was supported by National Institutes of Health grants to M.E.M. (AI 23598 and EY 11288) and M.G.R. (AI 11219). S.H. was supported by a National Institutes of Health postdoctoral fellowship (AI 060155).

REFERENCES

1. **Arnold, E., and M. G. Rossmann.** 1990. Analysis of the structure of a common cold virus, human rhinovirus 14, refined at a resolution of 3.0 Å. J. Mol. Biol. **211:**763–801.
2. **Arnold, K., L. Bordoli, J. Kopp, and T. Schwede.** 2006. The SWISS-MODEL workspace: a web-based environment for protein structure homology modeling. Bioinformatics **22:**196–201.
3. **Badger, J., I. Minor, M. J. Kremer, M. A. Oliveira, T. J. Smith, J. P. Griffith, D. M. A. Guerin, S. Krishnaswamy, M. Luo, M. G. Rossmann, M. A. McKinlay, G. D. Diana, F. J. Dutko, M. Fancher, R. R. Rueckert, and B. A. Heinz.** 1988. Structural analysis of a series of antiviral agents complexed with human rhinovirus 14. Proc. Natl. Acad. Sci. U. S. A. **85:**3304–3308.
4. **Belnap, D. M., B. M. McDermott, Jr., D. J. Filman, N. Cheng, B. L. Trus, H. J. Zuccola, V. R. Racaniello, J. M. Hogle, and A. C. Steven.** 2000. Three-dimensional structure of poliovirus receptor bound to poliovirus. Proc. Natl. Acad. Sci. U. S. A. **97:**73–78.
5. **Bergelson, J. M., J. G. Mohanty, R. L. Crowell, N. F. St. John, D. M. Lublin, and R. W. Finberg.** 1995. Coxsackievirus B3 adapted to growth in RD cells binds to decay-accelerating factor (CD55). J. Virol. **69:**1903–1906.
6. **Bergelson, J. M., M. P. Shepley, B. M. Chan, M. E. Hemler, and R. W. Finberg.** 1992. Identification of the integrin VLA-2 as a receptor for echovirus 1. Science **255:**1718–1720.
7. **Brodbeck, W. G., D. Liu, J. Sperry, C. Mold, and M. E. Medof.** 1996. Localization of classical and alternative pathway regulatory activity within the decay-accelerating factor. J. Immunol. **156:**2528–2533.
8. **Brünger, A. T., P. D. Adams, G. M. Clore, W. L. DeLano, P. Gros, R. W. Grosse-Kunstleve, J. S. Jiang, J. Kuszewski, M. Nilges, N. S. Pannu, R. J. Read, L. M. Rice, T. Simonson, and G. L. Warren.** 1998. Crystallography and NMR System: a new software suite for macromolecular structure determination. Acta Crystallogr. D Biol. Crystallogr. **54:**905–921.
9. **Clarkson, N. A., R. Kaufman, D. M. Lublin, T. Ward, P. A. Pipkin, P. D. MInor, D. J. Evans, and J. W. Almond.** 1995. Characterization of the echovirus 7 receptor: domains of CD55 critical for virus binding. J. Virol. **69:** 5497–5501.
10. **Collaborative Computational Project Number 4.** 1994. The CCP4 suite: programs for protein crystallography. Acta Crystallogr. D Biol. Crystallogr. **50:**760–763.
11. **Colonno, R. J., J. H. Condra, S. Mizutani, P. L. Callahan, M. E. Davies, and M. A. Murcko.** 1988. Evidence for the direct involvement of the rhinovirus canyon in receptor binding. Proc. Natl. Acad. Sci. U. S. A. **85:**5449–5453.
12. **Davis, I. W., A. Leaver-Fay, V. B. Chen, J. N. Block, G. J. Kapral, X. Wang, L. W. Murray, W. B. Arendall III, J. Snoeyink, J. S. Richardson, and D. C. Richardson.** 2007. MolProbity: all-atom contacts and structure validation for proteins and nucleic acids. Nucleic Acids Res. **35:**W375–W383.
13. **Filman, D. J., R. Syed, M. Chow, A. J. Macadam, P. D. MInor, and J. M. Hogle.** 1989. Structural factors that control conformational transitions and serotype specificity in type 3 poliovirus. EMBO J. **8:**1567–1579.
14. **He, Y., F. Lin, P. R. Chipman, C. M. Bator, T. S. Baker, M. Shoham, R. J. Kuhn, M. E. Medof, and M. G. Rossmann.** 2002. Structure of decay-accelerating factor bound to echovirus 7: a virus-receptor complex. Proc. Natl. Acad. Sci. U. S. A. **99:**10325–10329.
15. **Heeger, P. S., P. N. Lalli, F. Lin, A. Valujskikh, J. Liu, N. Muqim, Y. Xu, and M. E. Medof.** 2005. Decay-accelerating factor modulates induction of T cell immunity. J. Exp. Med. **201:**1523–1530.
16. **Heinz, B. A., R. R. Rueckert, D. A. Shepard, F. J. Dutko, M. A. McKinlay, M. Fancher, M. G. Rossmann, J. Badger, and T. J. Smith.** 1989. Genetic and molecular analyses of spontaneous mutants of human rhinovirus 14 that are resistant to an antiviral compound. J. Virol. **63:**2476–2485.
17. **Hofer, F., M. Gruenberger, H. Kowalski, H. Machat, M. Huettinger, E. Kuechler, and D. Blaas.** 1994. Members of the low density lipoprotein receptor family mediate cell entry of a minor-group common cold virus. Proc. Natl. Acad. Sci. U. S. A. **91:**1839–1842.
18. **Hourcade, D. E., L. Mitchell, L. A. Kuttner-Kondo, J. P. Atkinson, and M. E. Medof.** 2002. Decay-accelerating factor (DAF), complement receptor 1 (CR1), and factor H dissociate the complement AP C3 convertase (C3bBb) via sites on the type A domain of Bb. J. Biol. Chem. **277:**1107–1111.
19. **Icenogle, J. P., P. D. Minor, M. Ferguson, and J. M. Hogle.** 1986. Modulation of humoral response to a 12-amino-acid site on the poliovirus virion. J. Virol. **60:**297–301.
20. **Jones, T. A., M. Bergdoll, and M. Kjeldgaard.** 1990. O: a macromolecular modeling environment, p. 189–195. *In* C. Bugg and S. Ealick (ed.), Crystallographic and modeling methods in molecular design. Springer-Verlag Press, New York, NY.
21. **Jones, T. A., J. Y. Zou, S. W. Cowan, and M. Kjeldgaard.** 1991. Improved methods for building protein models in electron density maps and the location of errors in these models. Acta Crystallogr. A **47:**110–119.
22. **Kleywegt, G. J., and R. J. Read.** 1997. Not your average density. Structure **5:**1557–1569.
23. **Kolatkar, P. R., J. Bella, N. H. Olson, C. M. Bator, T. S. Baker, and M. G. Rossmann.** 1999. Structural studies of two rhinovirus serotypes complexed with fragments of their cellular receptor. EMBO J. **18:**6249–6259.
24. **Krissinel, E., and K. Henrick.** 2007. Inference of macromolecular assemblies from crystalline state. J. Mol. Biol. **372:**774–797.
25. **Kuhn, R. J., and M. G. Rossmann.** 2002. Interaction of major group rhinoviruses with their cellular receptor, ICAM-1, p. 85–91. *In* B. L. Semler and E. Wimmer (ed.), Molecular biology of picornaviruses. ASM Press, Washington, DC.
26. **Kuttner-Kondo, L., D. E. Hourcade, V. E. Anderson, N. Muqim, L. Mitchell, D. C. Soares, P. N. Barlow, and M. E. Medof.** 2007. Structure-based mapping of DAF active site residues that accelerate the decay of C3 convertases. J. Biol. Chem. **282:**18552–18562.
27. **Lalli, P. N., M. G. Strainic, M. Yang, F. Lin, M. E. Medof, and P. S. Heeger.** 2008. Locally produced C5a binds to T cell-expressed C5aR to enhance effector T-cell expansion by limiting antigen-induced apoptosis. Blood **112:** 1759–1766.
28. **Lea, S. M., R. M. Powell, T. McKee, D. J. Evans, D. Brown, D. I. Stuart, and P. A. van der Merwe.** 1998. Determination of the affinity and kinetic constants for the interaction between the human echovirus 11 and its cellular receptor, CD55. J. Biol. Chem. **273:**30443–30447.
29. **Liu, J., F. Lin, M. G. Strainic, F. An, R. H. Miller, C. Z. Altuntas, P. S. Heeger, V. K. Tuohy, and M. E. Medof.** 2008. IFN-gamma and IL-17 production in experimental autoimmune encephalomyelitis depends on local APC-T cell complement production. J. Immunol. **180:**5882–5889.
30. **Lukacik, P., P. Roversi, J. White, D. Esser, G. P. Smith, J. Billington, P. A. Williams, P. M. Rudd, M. R. Wormald, D. J. Harvey, M. D. Crispin, C. M. Radcliffe, R. A. Dwek, D. J. Evans, B. P. Morgan, R. A. Smith, and S. M. Lea.** 2004. Complement regulation at the molecular level: the structure of decay-accelerating factor. Proc. Natl. Acad. Sci. U. S. A. **101:**1279–1284.
31. **Martino, T. A., M. Petric, M. Brown, K. Aitken, C. J. Gauntt, C. D. Richardson, L. H. Chow, and P. P. Liu.** 1998. Cardiovirulent coxsackieviruses and the decay-accelerating factor (CD55) receptor. Virology **244:**302–314.
32. **Muckelbauer, J. K., M. Kremer, I. Minor, G. Diana, F. J. Dutko, J. Groarke, D. C. Pevear, and M. G. Rossmann.** 1995. The structure of coxsackievirus B3 at 3.5 Å resolution. Structure **3:**653–667.
33. **Nelsen-Salaz, B., H. J. Eggers, and H. Zimmermann.** 1999. Integrin $\alpha_v\beta_3$ (vitronectin receptor) is a candidate receptor for the virulent echovirus 9 strain Barty. J. Gen. Virol. **80:**2311–2313.
34. **Neumann, E., R. Moser, L. Snyers, D. Blaas, and E. A. Hewat.** 2003. A cellular receptor of human rhinovirus type 2, the very-low-density lipoprotein receptor, binds to two neighboring proteins of the viral capsid. J. Virol. **77:**8504–8511.
35. **Oberste, M. S., K. Maher, D. R. Kilpatrick, and M. A. Pallansch.** 1999. Molecular evolution of the human enteroviruses: correlation of serotype with VP1 sequence and application to picornavirus classification. J. Virol. **73:**1941–1948.
36. **Olson, N. H., P. R. Kolatkar, M. A. Oliveira, R. H. Cheng, J. M. Greve, A. McClelland, T. S. Baker, and M. G. Rossmann.** 1993. Structure of a human rhinovirus complexed with its receptor molecule. Proc. Natl. Acad. Sci. U. S. A. **90:**507–511.
37. **Otwinowski, Z., and W. Minor.** 1997. Processing of X-ray diffraction data collected in oscillation mode. Methods Enzymol. **276:**307–326.
38. **Pettigrew, D. M., D. T. Williams, D. Kerrigan, D. J. Evans, S. M. Lea, and D. Bhella.** 2006. Structural and functional insights into the interaction of echoviruses and decay-accelerating factor. J. Biol. Chem. **281:**5169–5177.
39. **Pevear, D. C., M. J. Fancher, P. J. Felock, M. G. Rossmann, M. S. Miller, G. Diana, A. M. Treasurywala, M. A. McKinlay, and F. J. Dutko.** 1989. Conformational change in the floor of the human rhinovirus canyon blocks adsorption to HeLa cell receptors. J. Virol. **63:**2002–2007.
40. **Powell, R. M., V. Schmitt, T. Ward, I. Goodfellow, D. J. Evans, and J. W. Almond.** 1998. Characterization of echoviruses that bind decay accelerating factor (CD55): evidence that some haemagglutinating strains use more than one cellular receptor. J. Gen. Virol. **79:**1707–1713.
41. **Powell, R. M., T. Ward, D. J. Evans, and J. W. Almond.** 1997. Interaction between echovirus 7 and its receptor, decay-accelerating factor (CD55): evidence for a secondary cellular factor in A-particle formation. J. Virol. **71:**9306–9312.
42. **Powell, R. M., T. Ward, I. Goodfellow, J. W. Almond, and D. J. Evans.** 1999. Mapping the binding domains on decay-accelerating factor (DAF) for haemagglutinating enteroviruses: implications for evolution of a DAF-binding phenotype. J. Gen. Virol. **80:**3145–3152.
43. **Rieder, E., A. E. Gorbalenya, C. Xiao, Y. He, T. S. Baker, R. J. Kuhn, M. G. Rossmann, and E. Wimmer.** 2001. Will the polio niche remain vacant? Dev. Biol. **105:**1–12.
44. **Rossmann, M. G.** 2000. Fitting atomic models into electron microscopy maps. Acta Crystallogr. D Biol. Crystallogr. **56:**1341–1349.
45. **Rossmann, M. G.** 1994. Viral cell recognition and entry. Protein Sci. **3:**1712–1725.

46. **Rossmann, M. G., and P. Argos.** 1975. A comparison of the heme binding pocket in globins and cytochrome b_5. J. Biol. Chem. **250:**7525–7532.
47. **Rossmann, M. G., E. Arnold, J. W. Erickson, E. A. Frankenberger, J. P. Griffith, H. J. Hecht, J. E. Johnson, G. Kamer, M. Luo, A. G. Mosser, R. R. Rueckert, B. Sherry, and G. Vriend.** 1985. Structure of a human common cold virus and functional relationship to other picornaviruses. Nature **317:** 145–153.
48. **Rossmann, M. G., R. Bernal, and S. V. Pletnev.** 2001. Combining electron microscopic with X-ray crystallographic structures. J. Struct. Biol. **136:**190–200.
49. **Rossmann, M. G., Y. He, and R. J. Kuhn.** 2002. Picornavirus-receptor interactions. Trends Microbiol. **10:**324–331.
50. **Rueckert, R. R.** 1990. Picornaviridae and their replication, p. 507–548. *In* B. N. Fields et al. (ed.), Fields virology, 2nd ed., vol. 1. Raven Press, New York, NY.
51. **Semler, B. L., and E. Wimmer (ed.).** 2002. Molecular biology of picornaviruses. ASM Press, Washington, DC.
52. **Shafren, D. R., D. J. Dorahy, R. A. Ingham, G. F. Burns, and R. D. Barry.** 1997. Coxsackievirus A21 binds to decay-accelerating factor but requires intercellular adhesion molecule 1 for cell entry. J. Virol. **71:**4736–4743.
53. **Sherry, B., A. G. Mosser, R. J. Colonno, and R. R. Rueckert.** 1986. Use of monoclonal antibodies to identify four neutralization immunogens on a common cold picornavirus, human rhinovirus 14. J. Virol. **57:**246–257.
54. **Smyth, M., T. Pettitt, A. Symonds, and J. Martin.** 2003. Identification of the pocket factors in a picornavirus. Arch. Virol. **148:**1225–1233.
55. **Stanway, G., P. Joki-Korpela, and T. Hyypiä.** 2000. Human parechoviruses—biology and clinical significance. Rev. Med. Virol. **10:**57–69.
56. **Strainic, M. G., J. Liu, D. Huang, F. An, P. N. Lalli, N. Muqim, V. S. Shapiro, G. R. Dubyak, P. S. Heeger, and M. E. Medof.** 2008. Locally produced complement fragments C5a and C3a provide both costimulatory and survival signals to naive CD4+ T cells. Immunity **28:**425–435.
57. **Stuart, A. D., H. E. Eustace, T. A. McKee, and T. D. K. Brown.** 2002. A novel cell entry pathway for a DAF-using human enterovirus is dependent on lipid rafts. J. Virol. **76:**9307–9322.
58. **Tam, P. E.** 2006. Coxsackievirus myocarditis: interplay between virus and host in the pathogenesis of heart disease. Viral Immunol. **19:**133–146.
59. **Tong, L., and M. G. Rossmann.** 1997. Rotation function calculations with GLRF program. Methods Enzymol. **276:**594–611.
60. **Uhrinova, S., F. Lin, G. Ball, K. Bromek, D. Uhrin, M. E. Medof, and P. N. Barlow.** 2003. Solution structure of a functionally active fragment of decay-accelerating factor. Proc. Natl. Acad. Sci. U. S. A. **100:**4718–4723.
61. **Uncapher, C. R., C. M. DeWitt, and R. J. Colonno.** 1991. The major and minor group receptor families contain all but one human rhinovirus serotype. Virology **180:**814–817.
62. **Verdaguer, N., I. Fita, M. Reithmayer, R. Moser, and D. Blaas.** 2004. X-ray structure of a minor group human rhinovirus bound to a fragment of its cellular receptor protein. Nat. Struct. Mol. Biol. **11:**429–434.
63. **Whitton, J. L., C. T. Cornell, and R. Feuer.** 2005. Host and virus determinants of picornavirus pathogenesis and tropism. Nat. Rev. Microbiol. **3:**765–776.
64. **Williams, D. T., Y. Chaudhry, I. G. Goodfellow, S. Lea, and D. J. Evans.** 2004. Interactions of decay-accelerating factor (DAF) with haemagglutinating human enteroviruses: utilizing variation in primate DAF to map virus binding sites. J. Gen. Virol. **85:**731–738.
65. **Williams, P., Y. Chaudhry, I. G. Goodfellow, J. Billington, R. Powell, O. B. Spiller, D. J. Evans, and S. M. Lea.** 2003. Mapping CD55 function. The structure of two pathogen-binding domains at 1.7 Å. J. Biol. Chem. **278:** 10691–10696.
66. **Xing, L., M. Huhtala, V. Pietiäinen, J. Käpylä, K. Vuorinen, V. Marjomäki, J. Heino, M. S. Johnson, and R. H. Cheng.** 2004. Structural and functional analysis of integrin α2I domain interaction with echovirus 1. J. Biol. Chem. **279:**11632–11638.
67. **Yan, X., R. S. Sinkovits, and T. S. Baker.** 2007. AUTO3DEM—an automated and high throughput program for image reconstruction of icosahedral particles. J. Struct. Biol. **157:**73–82.
68. **Zhang, P., S. Mueller, M. C. Morais, C. M. Bator, V. D. Bowman, S. Hafenstein, E. Wimmer, and M. G. Rossmann.** 2008. Crystal structure of CD155 and electron microscopic studies of its complexes with polioviruses. Proc. Natl. Acad. Sci. U. S. A. **105:**18284–18289.